Int. J. Electrochem. Sci., 17 **(2022)** Article Number: 220840, doi: 10.20964/2022.08.36

International Journal of
ELECTROCHEMICAL
SCIENCE
www.electrochemsci.org

Pt-doped FeP-C Hollow Nanorod and Hemoglobin Based Electrochemical Biosensor and Its Applications

Fan Shi[1], *Hui Cheng*[1], *Yucen Yao*[1], *Zejun Zhang*[1], *Lina Zeng*[2,*], *Lin Li*[2], *Wei Sun*[1,*]

[1] Key Laboratory of Water Pollution Treatment and Resource Rouse of Hainan Province, Key Laboratory of Functional Materials and Photoelectrochemistry of Haikou, College of Chemistry and Chemical Engineering, Hainan Normal University, Haikou 571158, P R China.
[2] Key Laboratory of Laser Technology and Optoelectronic Functional Materials of Hainan Province, College of Physics and Eletronic Engineering, Hainan Normal University, Haikou 571158, China
[*]E-mail: zenglinahainan@126.com (L.N. Zeng) and sunwei@hainnu.edu.cn (W. Sun)

Received: 5 May 2022 / *Accepted:* 11 June 2022 / *Published:* 4 July 2022

Sensitive detections of nitrite (NO_2^-), hydrogen peroxide (H_2O_2), bromate (BrO_3^-) and trichloroacetic acid (TCA) have very important significance in different fields. Herein, Pt-doped FeP-C hollow nanorod was fabricated by a controllable etching and in-situ carbonating procedure. Then, a modified electrode (Nafion/Hb/Pt-FeP-C/CILE) was constructed by dropping Pt-FeP-C, hemoglobin (Hb) and Nafion membrane on carbon ionic liquid electrode (CILE). Benefitting from the synergistic effects of Pt NPs and FeP-C, Pt-FeP-C provides a favorable biocompatible microenvironment for Hb attachment with enhanced catalytic performance. Electroanalysis of NO_2^-, H_2O_2, BrO_3^- and TCA were realized in the detection range from 0.2 to 7.0 mmol·L^{-1}, 0.3 to 7.0 mmol L^{-1}, 0.76 to 7.0 mmol·L^{-1}, 5.0 to 900.0 mmol L^{-1}, and the detection limits were 0.07 mmol L^{-1}, 0.1 mmol L^{-1}, 0.25 mmol L^{-1} and 1.67 mmol L^{-1}, respectively. The real samples were further analyzed with satisfactory results.

Keywords: Hemoglobin, Nitrite, Hydrogen peroxide, Bromate, Trichloroacetic acid, Electrochemical biosensor.

1. INTRODUCTION

Nitrite (eg. NO_2^-) is a commonly used food additive, which acts as antioxidant to the oxidation during treatment and storage [1]. However, the improper usage of nitrite in foods with higher carcinogenicity need more sensitive detection methods [2]. Hydrogen peroxide (H_2O_2) is important for regulating various metabolisms in biological systems, food industry and daily applications [3]. However, the residual H_2O_2 and its derived reactive species could cause oxidative damage to human health [4]. Bromate (BrO_3^-) is often regarded as an oxidant in the baking industry [5]. However, bromate is a chemical substance that could cause cancer as indicated by the International Agency for Research on

Cancer [6]. Trichloroacetic acid (TCA) is the most prevalent disinfection byproducts that is a potential valid biomarker for assessing chronic ingestion exposure from drinking water [7]. Many analytical techniques such as electrochemistry [8], chromatography [9], spectrophotometry [10], fluorimetry [11], and chemiluminescence [2] have been reported for these targets analysis, which have various specific properties. Enzyme-based biosensors use enzymes or microbial cells as biocatalysts for catalytic reactions, which have been used for the different analytes detection [12]. In our group, a series of enzyme electrochemical biosensors with horseradish peroxidase (HRP), myoglobin (Mb) and hemoglobin (Hb) [13-15] have been proposed with high sensitivity and selectivity. Besides, different kinds of nanomaterials have been used as the enhancer for enzyme electrodes [16-19]. Recently, metal-organic frameworks (MOFs) have been applied in catalysis, drug delivery, energy storage and sensing, with outstanding specific surface area, excellent porosity and thermal stability [20, 21]. MOFs and their derived materials have also been explored for the electrochemical sensors [22].

Herein, Pt-doped FeP-C was prepared with hollow nanorod structure by controllable etching and in-situ carbonating procedure. Furthermore, an Hb based electrochemical sensor was proposed with Pt-FeP-C, which could catalyze various substrates such as NO_2^-, H_2O_2, BrO_3^- and TCA. The fabrication of Nafion/Hb/Pt-FeP-C/CILE based electrochemical biosensor was shown in Scheme 1.

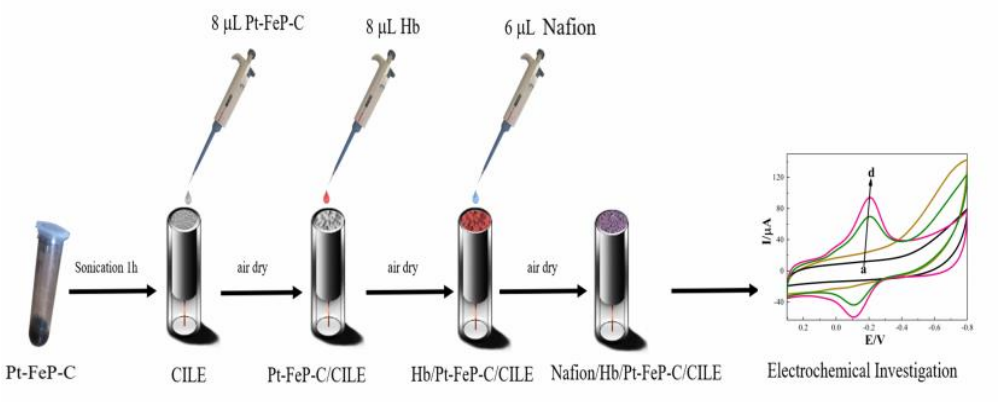

Scheme 1. Fabrication of Nafion/Hb/Pt-FeP-C/CILE based electrochemical sensor.

2. EXPERIMENTAL

2.1. Reagents

$Fe(NO_3)_3{\cdot}9H_2O$, K_2PtCl_6, fumaric acid ($C_4H_4O_4$), hemoglobin (Hb), ionic liquid (IL) N-hexylpyridine hexafluorophosphate ($HPPF_6$), $KBrO_3$, TCA, H_2O_2, and $NaNO_2$ were obtained from Aladdin Reagent Co., Ltd. (Shanghai, China). Phosphate buffer solution (PBS, 0.1 mol L^{-1}) was used as electrolyte, and N_2 was used for deoxygenation of the buffer solution. Ultrapure water filtered by Milli-Q IQ 7000 purification system (Merck Millipore, Germany) was used throughout the experiment and other chemicals used were of analytical grade.

2.2. Apparatus

X-ray photoelectron spectroscopy (XPS) was performed for the elemental analysis on ESCALAB 250 X-ray photoelectron spectrometer (Thermo Electron, USA) with a monochromatic Al Kα (1486.6 eV) source. Ultraviolet-visible (UV-Vis) absorption spectrum was obtained from UV-5 spectrophotometer (Mettler Toledo, USA). Fourier transform infrared (FT-IR) was measured by Nicolet 6700 FT-IR spectrometer (Thermo Fisher Technologies, USA). Morphology of the materials was observed using JSM-7100F scanning electron microscope (Japan Electron Co. Ltd., Japan). Electrochemical measurements were performed on CHI 660E electrochemical workstation (Shanghai CH Instrument Co. Ltd., China) with a three-electrode system including the laboratory self-made Nafion/Hb/Pt-FeP-C/CILE (φ = 4.0 mm) as the working electrode, saturated calomel electrode (SCE) as the reference electrode, and platinum electrode as the auxiliary electrode.

2.3 Material synthesis

Based on the reference [23], 0.2786 g $C_4H_4O_4$ was added into water and heated at 70 ℃ with stirring to get a clarified solution. Then, 1.05 g $Fe(NO_3)_3·9H_2O$ was added to the solution under agitation until complete dissolution. Finally, the resulting solution was poured into a Teflon-lined stainless steel autoclave, and heated at 110 ℃ for 6 h. The resulted product was washed with water and ethanol, and then dried at 60 ℃ in a vacuum oven to obtain the precursor Mil-88A (Fe) nanorods. Subsequently, Mil-88A (Fe) nanorods doped with Pt were prepared by the similar method by adding 0.015 mmol K_2PtCl_6 to the solution.

100 mg precursor Mil-88A (Fe) or Pt-Mil-88A (Fe) nanorods were completely dispersed in 10 mL water by magnetic agitation. During stirring, 15 mL 0.1 mol L^{-1} phytic acid solution was dropped and kept in a 90 ℃ water bath for 4 h. After cooling, it was centrifuged, washed, and finally dried to get the white solid, which were put in a tubular furnace and heated at 200 ℃ for 2 h, then heated at 900 ℃ for 2 h under N_2 protection at a heating rate of 2 ℃ min^{-1}. After natural cooling, Pt-FeP-C nanorod was obtained.

2.4 Electrodes preparation

IL is valuable to electrochemistry with the eminent qualities such as low metaling point, tremendous electrical conductivity, which can be used to fabricate CILE with good stability. Herein, IL $HPPF_6$ and graphite powder was utilized to fabricate CILE based on typical procedure [24]. Then, 8.0 μL Pt-FeP-C ethanol suspension (1.0 mg mL^{-1}) solution was casted onto the CILE surface and dried at 25 ℃ to obtain Pt-FeP-C/CILE. Then, Hb/Pt-FeP-C/CILE was obtained by dropping 8.0 μL Hb solution (15.0 mg mL^{-1}) on Pt-FeP-C/CILE, and after dried, Nafion/Hb/Pt-FeP-C/CILE was obtained by dropping 6.0 μL 0.5% Nafion ethanol solution. The contrast electrodes, such as Nafion/CILE, Nafion/Hb/CILE and Nafion/Pt-FeP-C/CILE were also prepared by similar steps.

3. RESULTS AND DISCUSSION

3.1 SEM and TEM characterizations

SEM images of Pt-FeP-C at different magnifications (Fig. 1A and B) indicated that Pt-FeP-C had a uniform and porous loose structure with a hollow rod-like structure observed through the broken edge of nanorods. This structure possesses large effective surface area and could better bond with proteins, which is mainly attributed to acid etching and carbonized by high temperature. TEM image (Fig. 1C) further proves that Pt-FeP-C has specific hollow rod-like structure.

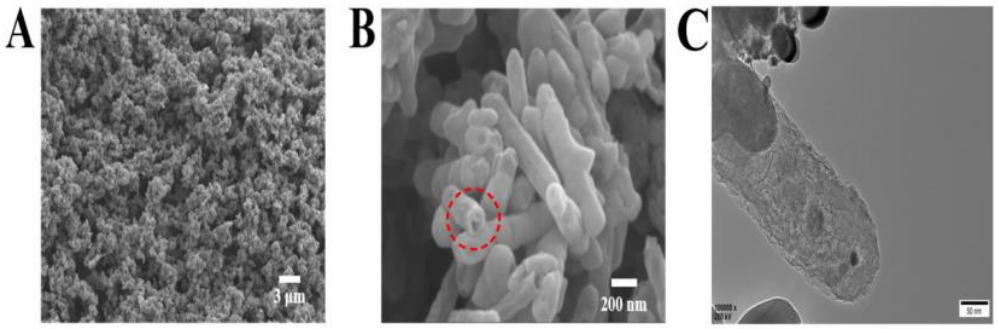

Figure 1. SEM images (A and B) and TEM image (C) of Pt-FeP-C.

3.2 Spectral characterizations

XPS were investigated and shown in Fig. 2, which could display the surface species and electronic states of Pt-FeP-C. As shown in Fig. 2A, full spectrum proves the existence elements including Fe, P, Pt, and C. A pair of peaks at 133.92 eV and 134.62 eV in P 2p spectrum (Fig. 2B) are originated from phosphate, caused by the oxidization of O_2 in air. In high-resolution spectrum of Fe 2p (Fig. 2C), the peak with binding energy of 709.58 eV is assigned to Fe-P. The peaks at 711.58 eV and 713.58 eV are associated with Fe $2p^{3/2}$, and the peaks located at 723.98 eV and 725.88 eV are associated with Fe $2p^{1/2}$. In the region of Pt 4f, two distinct peaks (Pt $4f^{7/2}$ and Pt $4f^{5/2}$) are assigned to Pt^0 and Pt^{2+} (Fig. 2D), which indicates that the Pt NPs doped on FeP-C are metallic state.

UV-Vis spectroscopy was performed to check the structure of heme proteins based on the Soret absorption bands, which provides detailed results about structure of Hb. The Soret absorption band of Hb within Pt-FeP-C appeared at 405.4 nm (Fig. 2E, curve b), and it is same as that of pure Hb (Fig. 2E, curve a), therefore Mb keeps the secondary structure and conformational integrity in the native state. It also proved that Pt-FeP-C do not influence fundamental active conformation of Hb [15]. In addition, FT-IR spectra were checked to verify the polypeptide chain of Hb (Fig. 2F). The amide I (1648.92 cm^{-1}) and the amide II band (1548.64 cm^{-1}) of Hb are also same as the essential native structure within in the mixture of Pt-FeP-C nanorods, indicating the undenaturation of the Hb molecules [15].

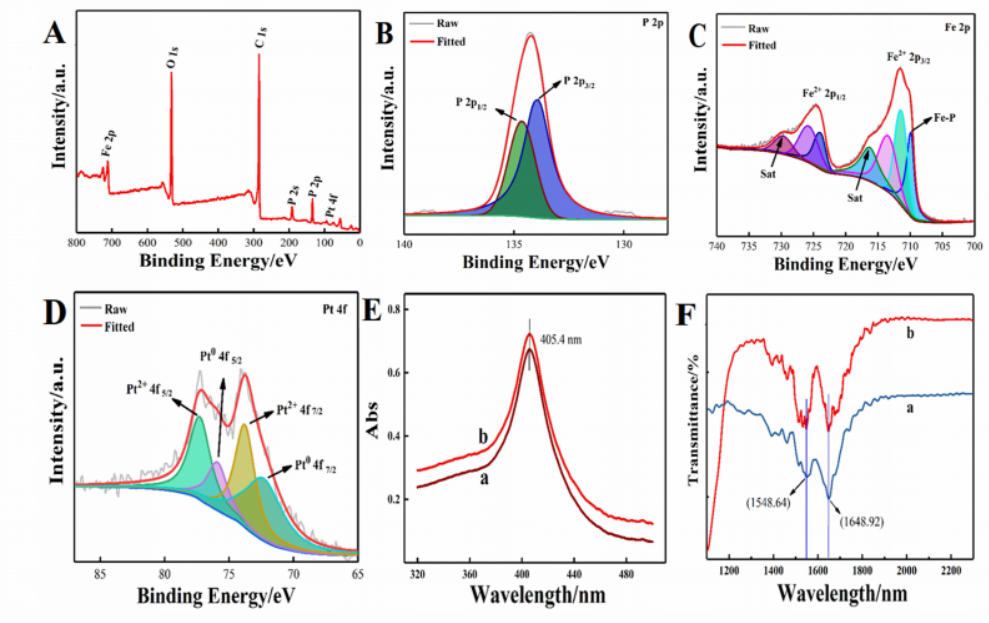

Figure 2. (A) XPS full spectrum of Pt-FeP-C; (B) P 2p; (C) Fe 2p; (D) Pt 4f; (E) UV-Vis absorption spectrum of (a) Hb solution and (b) Hb@Pt-FeP-C mixed solution; (F) FT-IR spectra of (a) Hb and (b) Hb@Pt-FeP-C mixture.

3.3 Electrochemical characterizations

Cyclic voltammetric (CV) responses of various working electrodes in $[Fe(CN)_6]^{3-}$ solution was studied and shown in Fig. 3A, in which redox peak current increased greatly from Nafion/CILE to Nafion/Pt-FeP-C/CILE, proving the positive effect of Pt/FeP-C on the working electrode. CVs of Nafion/Pt-FeP-C/CILE with the increase of scan rates (υ) were recorded (Fig. 3B), which could be used to calculate the electrochemical active surface area (ECSA) of the electrode according to the Randles-Sevcik equation [25]. The linear relationships between *I*p and $\upsilon^{1/2}$ on Nafion/Pt-FeP-C/CILE are *I*pc (μA) = 535.733 $\upsilon^{1/2}$ + 22.970 (n = 12, γ = 0.999) and *I*pa (μA) = -549.263 $\upsilon^{1/2}$-21.341 (n = 12, γ = 0.999). Then, the ECSA of Nafion/Pt-FeP-C/CILE is got as 0.723 cm^2, much larger than that of Nafion/CILE (0.339 cm^2). These results indicate Pt-FeP-C composite could greatly enhance the ECSA on the working electrode.

CV was further performed to evaluate the electrochemical responses of Hb at four working electrodes in PBS (pH 2.0) (Fig. 3C). Notably, no response on Nafion/CILE (curve a) or Nafion/Pt-FeP-C/CILE (curve b) was due to no Hb present on the electrodes. By contrast, two small redox peaks were observed on Nafion/Hb/CILE (curve c), indicating the direct electrochemical reaction of Hb on the surface of the electrode. The redox peak currents on Nafion/Hb/Pt-FeP-C/CILE (curve d) increased drastically, which was primarily because the enhanced electron transport by Pt-FeP-C. The cathodic (E_{pc}) and anodic (E_{pa}) peak potentials at -0.205 V and -0.108 V was used to calculate the formal peak potential ($E^{0'}$) from the average of E_{pc} and *E*pa with the result as -0.157 V (vs. SCE), a typical value of Fe^{III}/Fe^{II} in heme groups [26]. The peak-to-peak potential (ΔEp, 97 mV) and the value of I_{pc}/I_{pa} (1.2) further proved a quasi-reversible process. This redox peak is originated from the electrical center of Hb and the

higher peak current is attributed to Pt-FeP-C with large specific surface area, excellent conductivity and biocompatibility.

The influence of buffer pH on CV responses of Nafion/Hb/Pt-FeP-C/CILE was recorded in the pH range (2.0 to 6.0) (Fig. 3D). As can be seen, $E^{0'}$ was gradually moved to the negative direction with increasing PBS pH, which was due to protons took part in the reaction. Moreover, a good linear relationship (Fig. 3E) of $E^{0'}$ *vs* pH was plotted as $E^{0'}$(V) = −0.044 pH− 0.109 (n = 5, γ = 0.999). The slope value of -44.0 mV pH^{-1} and the theoretical value of -59.0 mV pH^{-1} are close, which proves that the transfer process is single proton coupled electron. The highest redox current was attained at pH 2.0, therefore pH 2.0 was optimal pH (Fig. 3F).

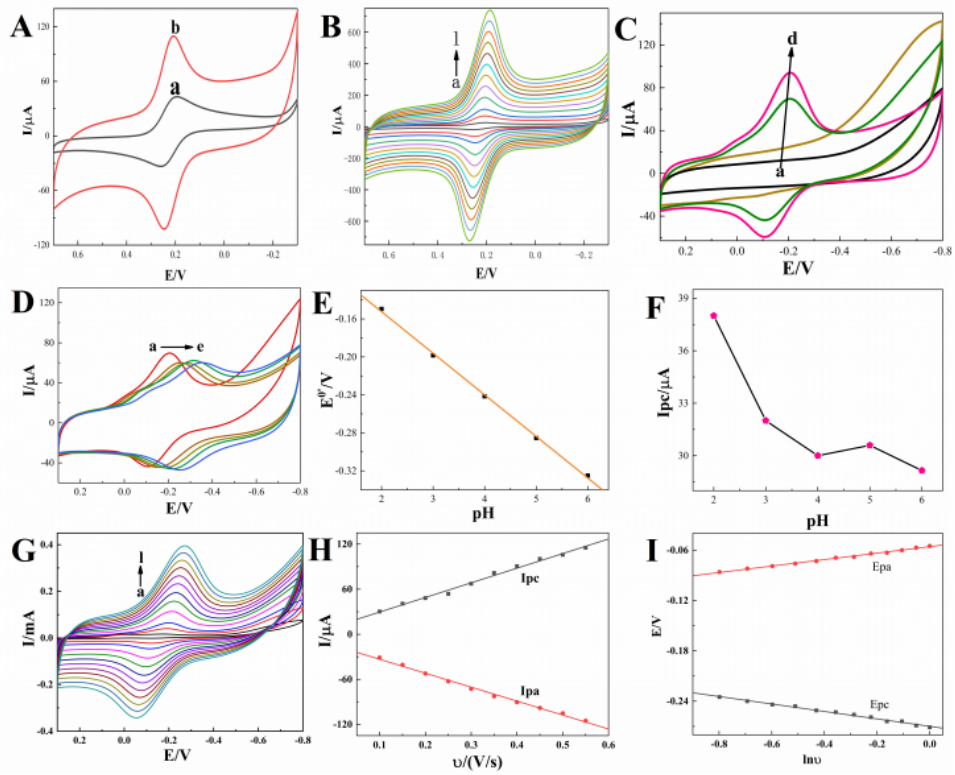

Figure 3. (A) CVs of different electrodes (a) Nafion/CILE and (b) Nafion/Pt-FeP-C/CILE in 1.0 mmol L^{-1} $K_3[Fe(CN)_6]$ and 0.50 mol L^{-1} KCl; (B) Influence of scan rate on CV response of Pt-FeP-C with scan rates from a to l as 0.01, 0.05, 0.10, 0.20, 0.30, 0.40, 0.50, 0.60, 0.70, 0.80, 0.90, 1.00 V s^{-1} in 1.0 mmol L^{-1} $K_3[Fe(CN)_6]$ and 0.50 mol L^{-1} KCl; (C) CVs of Hb at different electrodes (a) Nafion/CILE, (b) Nafion/Pt-FeP-C/CILE, (c) Nafion/Hb/CILE, and (d) Nafion/Hb/Pt-FeP-C/CILE in pH 2.0 PBS with scan rate as 0.10 V s^{-1}; (D) Influence of pH on CV response of Nafion/Hb/Pt-FeP-C/CILE in PBS (a to e: pH 2.0, 3.0, 4.0, 5.0, 6.0); (E) The linear relationship between $E^{0'}$and pH; (F) Relationship between *I*pc and pH; (G) CVs of Nafion/Hb/Pt-FeP-C/CILE at different scan rates (from a to l are 0.01, 0.05, 0.10, 0.20, 0.30, 0.40, 0.50, 0.60, 0.70, 0.80, 0.90, 1.00 V s^{-1}); (H) Linear relationship of *I*p *vs* υ; (I) Linear relationship of *E*p *vs* lnυ.

CV responses were performed to study the influence of scan rate on Nafion/Hb/Pt-FeP-C/CILE (Fig. 3G). Two well-defined linear lines (Fig. 3H) were got from 10 to 1000 mV s^{-1} with the linear regression equations as *I*pc (μA) = 194.606 υ (V s^{-1}) + 10.155 (n = 10, γ = 0.991) and *I*pa (μA) = –

186.715 υ (V s^{-1}) – 14.752 (n = 10, γ = 0.995), indicating a typical surface-controlled electrochemical behavior. The linear relationship (Fig. 3I) between *E*p and lnυ were got as *E*pc (V) = –0.044 lnυ (V s^{-1}) – 0.270 (n = 12, γ = 0.990) and *E*pa (V) = 0.039 lnυ (V s^{-1}) – 0.056 (n = 12, γ = 0.995). Moreover, the values of the electron transfer number (*n*), the charge transfer coefficient (*α*) and the apparent heterogeneous electron transfer rate constant (k_s) were calculated as 1.244, 0.465 and 1.666 s^{-1}, respectively, according to Laviron's equation [27]. Due to specific properties of Pt-FeP-C on the working electrode, the k_s value of 1.666 s^{-1} was larger than that of 1.22 s^{-1} on Nafion/Mb/Au-BC/CILE [14], 1.12 s^{-1} on Nafion/Hb/HGNs/CILE [26], 1.13 s^{-1} on Nafion/Hb/ZnO-CNF/CILE [15], and 0.690 s^{-1} on Nafion/Hb/MgO@CNFs/CILE [19].

3.4 Electrocatalytic activity

CV responses was performed to investigate the electrocatalytic performance of Nafion/Pt-FeP-C/CILE towards NO_2^- (Fig. 4A). When NO_2^- was added in PBS, a new reduction peak at –0.560 V was observed and the reduction peak current was linearly increased with the concentration of NO_2^- from 0.2 to 1.7 mmol L^{-1} and 1.7 to 7.0 mmol L^{-1}. The reduction peak reached a plate-current value after the concentration of NO_2^- larger than 7.0 mmol L^{-1}. Two linear curves were obtained as *I*pc (μA) = 137.604 C (mmol L^{-1}) – 2.962 (n = 8, γ = 0.994) and *I*pc (μA) = 36.794 C (mmol L^{-1}) + 165.396 (n = 7, γ = 0.991), with the detection limit as 0.67 mmol·L^{-1} (3σ). Besides, from the Lineweaver–Burk equation [28], the Michaelis–Menten constant (K_M^{app}) was got as 1.13 mmol·L^{-1}, which was much lower than that on Nafion/Mb/Au-BC/CILE (7.14 mmol·L^{-1}) [14], Nafion/HRP/AuNPs-CCNTs/CILE (7.66 mmol·L^{-1}) [29] and BP-PEDOT: PSS-hemin/CILE (8.95 mmol·L^{-1}) [30]. The lower K_M^{app} could prove the higher biological affinity of the modified electrode surface to NO_2^-.

Electrocatalytic reduction of H_2O_2 on Nafion/Pt-FeP-C/CILE was shown in Fig. 4B. When H_2O_2 was added in the PBS, the reduction peaks were enhanced, whereas the oxidation currents completely disappeared due to the Hb-catalyzed reduction of H_2O_2. Nafion/Pt-FeP-C/CILE exhibited a good linear relationship to H_2O_2 concentration from 0.3 to 7.0 $mmol^{-1}$ with the regression equation as *I*pc (μA) = 8.227 C (mmol L^{-1}) + 15.808 (n = 12, γ = 0.996), and the detection limit of 0.01 mmol·L^{-1} (3σ). The K_M^{app} was got as 0.82 mmol L^{-1}, which was much smaller than that on Nafion/Hb/GQD/ CILE (25.32 mmol L^{-1}) [31] and BP-PEDOT: PSS-hemin/CILE (11.09 mmol L^{-1}) [30]. This lower K_M^{app} indicated that Nafion/Pt-FeP-C/CILE had a better biological affinity to H_2O_2.

Electrocatalysis of Nafion/Pt-FeP-C/CILE to BrO_3^- from 0.76 to 40.0 mmol L^{-1} and 4.0 to 7.0 mmol L^{-1} was shown in Fig. 4C. A new reduction peak appeared at –0.221 V with increasing concentration of BrO_3^-, meanwhile, the reduction peak current increased and the potential moved negatively (curves a-o). Two linear equations can be obtained as *I*pc (μA) = 4.827 C (mmol L^{-1}) + 25.369 (n = 7, γ = 0.996) and *I*pc (μA) = 2.396 C (mmol L^{-1}) + 0.083 (n = 14, γ = 0.995). The detection limit was calculated to be 0.267 mmol L^{-1}(3σ), and the K_M^{app} was 0.59 mmol L^{-1}. This K_M^{app} was much lower than the previous results, such as 6.08 mmol L^{-1}on Mb-CA-graphene microspheres [29].

In Fig. 4D, electrocatalytic reduction of TCA is recorded with a new reduction peak at –0.475 V. Nafion/Pt-FeP-C/CILE exhibited an excellent linear response to TCA concentration from 5.00 to 900.00 mmol L^{-1} with the equation as *I*pc (μA) = 1.337 C (mmol L^{-1}) + 17.015 (n = 23, γ = 0.998), and the

detection limit as 1.67 mmol L^{-1}. When the TCA concentration was more than 900.0 mmol L^{-1}, the catalytic current almost stayed invariant and the K_M^{app} was calculated as 6.91 mmol L^{-1}, which is smaller than the previous sensors, such as Nafion/Mb/Au−BC/CILE (78.5 mmol L^{-1}) [14], Nafion/Hb/GQD/CILE (50.4 mmol L^{-1}) [32], and BP-PEDOT: PSS-hemin/CILE (14.3 mmol L^{-1}) [28]. Comparison of analytical performances of various modified electrodes was listed in Table 1.

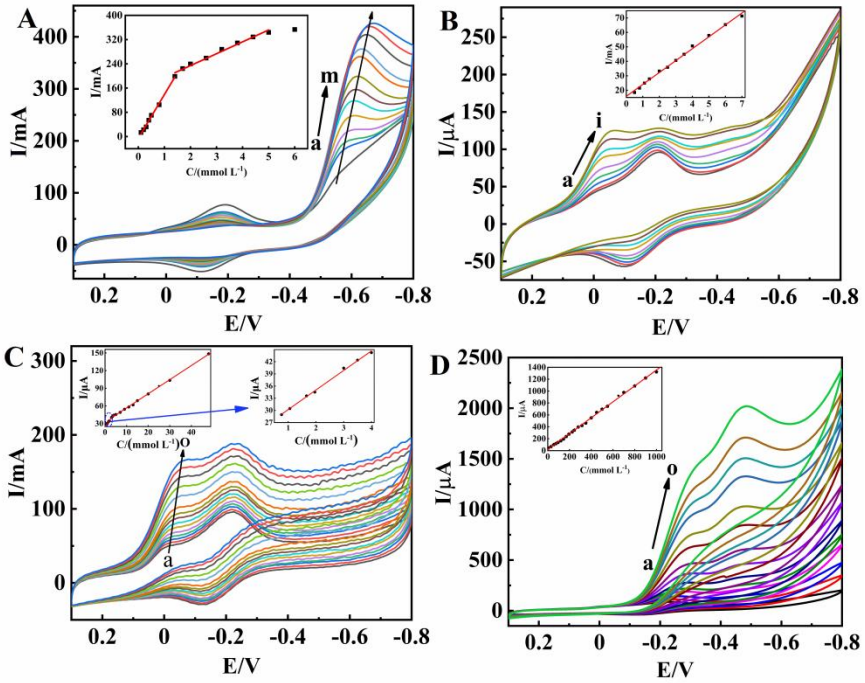

Figure 4. CVs of Nafion/Hb/Pt-FeP-C/CILE with different concentrations of (A) NO_2^- (from a to m: 0.20, 0.50, 0.80, 1.10, 1.40, 1.70, 2.00, 2.60, 3.20, 3.80, 5.00, 6.00, 7.00 mmol L^{-1}), inset is the linear relationship of *I vs* C (NO_2^-); (B) H_2O_2 (from a to i: 0.30, 0.50, 0.80, 1.40, 2.00, 3.00, 4.00, 5.00, 7.00 mmol L^{-1}), inset is the linear relationship of *I vs* C (H_2O_2); (C) BrO_3^- (from a to o: 0.76, 1.40, 2.00, 3.00, 4.00, 5.00, 7.00, 9.00, 11.00, 13.00, 15.00, 20.00, 25.00, 30.00, 40.00 mmol L^{-1}), inset is the linear relationship of *I vs* C (BrO_3^-); (D) TCA (from a to o: 5.00, 25.00, 55.00, 95.00, 120.00, 170.00, 225.00, 330.00, 400.00, 500.00, 600.00, 700.00, 800.00, 900.00 mmol L^{-1}), inset is the linear relationship of *I vs* C (TCA).

3.5 Reproducibility and stability

Stability and reproducibility are important indicators to measure whether electrodes can be accurately measured and used effectively. Firstly, the reproducibility with ten Nafion/Hb/Pt-FeP-C/CILE electrodes was evaluated by CV in PBS with 5.0 mmol·L^{-1} NO_2^-. The relative standard deviation (RSD) was 3.25%, indicating an excellent reproducibility. Furthermore, the long-term stability of the proposed sensor was tested in a 30-day period storing the modified electrodes at 4 °C, CV responses retained 94.07% of the initial current and the RSD value was 4.32%, indicating a good stability.

Table 1. Comparison of analytical performances of various modified electrodes.

Electrodes	Analyte	Linear range (mmol L^{-1})	LOD (mmol L^{-1})	K_M^{app} (mmol L^{-1})	Refs
Nafion/Mb/Au−BC/CILE	TCA	4.0-240.0	1.33	78.5	[14]
	NO_2^-	1.0-30.0	0.33	7.14	
Nafion/HRP/AuNPs-CCNTs/CILE	BrO_3^-	0.5-10.0	0.16	6.08	[29]
	NO_2^-	0.1-0.9; 0.9-3.0	0.03	7.66	
Hb/AgNF/ITO	H_2O_2	0.2 - 3.4	0.12	0.63	[31]
	NO_2^-	1.0-10.5	0.033	8.95	
	TCA	4.0-35.0	1.33	14.30	
Nafion/Hb/GQD/ CILE	TCA	6.0-100.0	2.0	50.4	[32]
	NO_2^-	2.0-12.0	0.67	1.13	
	H_2O_2	6.0-30.0	2.0	25.32	
Hemin-MIL-88-NH_2/CNT	H_2O_2	0.5×10^{-3}-0.203	0.06×10^{-3}	-	[33]
Mb-CA-graphene microspheres	H_2O_2	8.0-100.0	1.05×10^{-3}	-	[34]
	NO_2^-	1.5-17.5	0.15	-	
Nafion/Hb/Pt-FeP-C/CILE	TCA	2.5-27.5	2.05	0.27	This work
	NO_2^-	0.20-7.00	0.07	1.13	
	H_2O_2	0.30-7.00	0.10	0.82	
	BrO_3^-	0.76-7.00	0.25	0.59	
	TCA	5.00~900	1.67	6.91	

Note: Mb: myoglobin; BC: porous biomass carbon; Au: gold; ITO: indium tin oxide; CA: calcium alginate; HRP: horseradish peroxidase; CCNTs: coiled carbon nanotubes; GQD: graphene quantum dots; BPE: black phosphorene.

3.6 Practical Applications

To validate the applicability of the proposed sensor in real samples, NO_2^- and H_2O_2 in pickled vegetables samples (Haikou Guilinyang market, China) and 3.0% medical H_2O_2 (Guangdong Nanguo Pharmaceutical Co., Ltd.) were determined, respectively. Pickled vegetables sample was treated with the following procedure. Firstly, the pickled vegetables samples were cut into small pieces and soaked in water for 3 hours. Then the socked water was strained through 0.45 μm filter to obtain the sample solution. CV responses with the calibration curves for the detection of NO_2^- concentration for three parallel detections in the sample. Three repetitive measurements were made for each sample by the standard addition method. Moreover, 3.0% medical H_2O_2 was tested by the similar procedure. The recovery was in the range from 92.00% to 102.00% (shown in Table 2), demonstrating the practical applications with a good detection effect.

Table 2. Analysis results of NO_2^- and H_2O_2 in real samples (n=3).

Target	Samples	Detected (mmol L^{-1})	Added (mmol L^{-1})	Total (mmol L^{-1})	Recovery (%)	RSD (%)
NO_2^-	Soak water from pickled vegetables	3.93	1.00	4.85	92.00	2.06
			2.00	5.94	100.50	1.98
			3.00	6.95	100.67	2.57
H_2O_2	3.0 % Medical H_2O_2	1.57	1.00	2.59	102.00	3.35
			2.00	3.52	97.50	3.69
			3.00	4.61	101.33	4.12

4. CONCLUSION

Sum up, an electrochemical sensor was developed and used for the electrocatalysis of NO_2^-, H_2O_2, BrO_3^- and TCA. Herein, Pt NPs decorated FeP-C hollow nanorod was synthesized and exhibited an excellent microenvironment for loading Hb with stable catalytic activity. Satisfactory results in the comparison of analytical performances with the previous reports verified the usage of Pt-FeP-C in electrochemical sensors with the advantages such as excellent conductivity and the synergistic effects. Due to the high biological affinity to NO_2^-, H_2O_2, BrO_3^- and TCA, the sensor had the advantages of high sensitivity and rapid response for the real applications.

ACKNOWLEDGEMENTS
This work is supported by Hainan Provincial Natural Science Foundation (2019RC190), Science and Technology project of Hainan Province (ZDYF2020217), Scientific Research Projects of Higher Education Institutions in Hainan Province (Hnky2020ZD-12), the Open Foundation of Key Laboratory of Laser Technology and Optoelectronic Functional Materials of Hainan Province (2022LTOM02).

References

1. P. Miao, Z. Liu, J. Guo, M. Yuan, R. Zhong, L. Wang and F. Zhang, *RSC Adv.*, 9 (2019) 17698.
2. Z. Yan, Z. Zhang, Y. Yu, Z. Liu and J. Chen, *Food Chem.*, 190 (2016) 20.
3. L. Xing, W. Zhang, L. Fu, J.M. Lorenzo and Y. Hao, *Food Chem.*, 385 (2022) 132555.
4. W. Chen, S. Cai, Q.Q. Ren, W. Wen and Y.D. Zhao, *Analyst*, 137 (2012) 49.
5. V. Shanmugavel, K. Komala Santhi, A.H. Kurup, S. Kalakandan, A. Anandharaj and A. Rawson, *Food Chem.*, 311 (2020) 125964.
6. M. El Ati-Hellal, R. Doggui, Y. Krifa and J. El Ati, *Environ. Sci. Pollut. Res. Int.*, 25(2018)2702.
7. Y. Hu, L. Tan, S.H. Zhang, Y.T. Zuo, X. Han, N. Liu, W.Q. Lu and A.L. Liu, *Environ. Sci. Pollut. Res. Int.*, 24 (2017) 1509.
8. B. Shao, W. Chen, L.J. Yan, Y.H. Huang, B. Wang, Q.W. Zou, Y.K. Xuan, W. Sun and Y.Y. Niu, *Int. J. Electrochem. Sci.*, 16 (2021) 211039.
9. M.G. Pervova, V.E. Kirichenko and K.I. Pashkevich, *J. Anal. Chem.*, 57 (2002) 326.
10. H. Wang, N. Wan, L. Ma, Z. Wang, B. Cui, W. Han and Y. Chen, *Analyst*, 143 (2018) 4555.
11. M. Li, P. Lei, S. Song, S. Shuang and C. Dong, *Analyst*, 146 (2021) 509.
12. Neelam, A.K. Chhillar and J.S. Rana, *Anal. Biochem.*, 581 (2019) 113345.
13. Y.Y. Niu, R.Y. Zou, H.A. Yones, X.B. Li, X.Y. Li, X.L. Niu, Y. Chen, P. Li and W. Sun, *J. Chin. Chem. Soc.*, 65 (2018) 1127.
14. F. Shi, L.J. Yan, X.Q. Li, C.L. Feng, C.Z. Wang, B.X. Zhang and W. Sun, *J. Chin. Chem. Soc.*, 68 (2021) 2006.

15. L. Zhu, X. Li, Y. Deng, R. Zou, B. Shao, L. Yan, C.X. Ruan, G.J. Li and W. Sun, *J. Iran. Chem. Soc.*, 18 (2020) 1027.
16. H. Xie, G.L. Luo, Y.Y. Niu, W.Z. Weng, Y.X. Zhao, Z.Q. Ling, C. Ruan, G.J. Li and W. Sun, *Mater. Sci. Eng. C*, 107 (2020) 110209.
17. Y. Deng, Z.R. Wen, G.L. Luo, H. Xie, J. Liu, Y.R. Xi, G.J. Li and W. Sun, *Curr. Anal. Chem.*, 16 (2020) 703.
18. Y.Y. Niu, X.Y. Li, H. Xie, G.L. Luo, R.Y. Zou, Y.R. Xi, G.J. Li and W. Sun, *J. Chin. Chem. Soc.,* 67 2019) 1054.
19. H. A. Yones, L. Zhu, B. Shao, S. Zhang, H. Xie, X.Q. Li and W. Sun, *Int. J. Electrochem. Sci*., 16 (2021) 211039.
20. M. Farrag, *Microporous Mesoporous Mater.*, 312 (2021) 110783.
21. X. Qiao, X. Ma, X. Ma, T. Yue and Q. Sheng, *Sens. Actuators B Chem.*, 334 (2021) 129682.
22. G.L. Luo, Y. Deng, X.P. Zhang, R.Y. Zou, W. Sun, B.H. Li, B. Sun, Y.B. Wang and G.J. Li, *New J. Chem.*, 43 (2019) 16819.
23. Y. Deng, Z.Y. Xiao, Z.C. Wang, J.P. Lai, X.B. Liu, D. Zhang, Y. Han, S.X. Li, W. Sun and L. Wang, *Appl. Catal. B Environ.*, 291 (2021) 120047.
24. L.J. Yan, L.F. Huang, T.X. Hu, Y.J. Ai, B. Wang and W. Sun, *Talanta*, 242 (2022) 123295.
25. A.J. Brad and L.R. Faulkner, Electrochemical Methods: Fundamentals and Applications, Wiley, (2000) New York, USA.
26. X.Q. Li, B. Shao, Y.X. Sun, B.X. Zhang, X.H. Wang, W. Sun, *Int. J. Electrochem. Sci.*, 16 (2021) 210219.
27. E. Laviron, *J. Electroanal. Chem. Interfacial Electrochem.*, 52 (1974) 355.
28. R.A. Kamin and G.S. Wilson, *Anal. Chem.,* 52 (1980) 1198.
29. Y.C. Yao, C.X. Yin, S.G. Xu, M. Jiang, L. Zhu, R.Y. Zou and W. sun, *Int. J. Electrochem. Sci.*, 17 (2022) 220546.
30. X.Y. Li, G.L. Luo, H. Xie, Y.Y. Niu, X.B. Li, R.Y. Zou, Y. Xi, Y. Xiong, W. Sun and G.J. Li, *Mikrochim. Acta*, 186 (2019) 304.
31. A.K. Yagati, H.T. Ngoc Le and S. Cho, *Nanomaterials-Basel*, 10 (2020) 1628.
32. X. Li, H. Xie, G.L. Luo, Y.Y. Niu, X.B. Li, Y.R. Xi, Y. Xiong, Y. Chen and W. Sun, *Curr. Anal. Chem.*, 16 (2020) 308.
33. J. Ji, S.Y. Ko, K.M. Choi and Y. Kwon, *Appl. Surf. Sci.*, 554 (2021) 148786.
34. C. Yu, H. Sun and S. Hou, *Anal. Methods*, 9 (2017) 4873.